PHYSICAL REVIEW C VOLUME 40, NUMBER 4 OCTOBER 1989

Excitation energy equilibration in damped ^{139}La+^{40}Ar collisions at 15 MeV per nucleon

J. L. Wile, S. S. Datta, W. U. Schröder, J. R. Huizenga, R. T. de Souza, and D. Pade
Departments of Chemistry and Physics and Nuclear Structure Research Laboratory,
University of Rochester, Rochester, New York 14627

(Received 3 April 1989)

Energy and angular distributions of neutrons emitted in coincidence with projectile-like fragments from the damped reaction ^{139}La+^{40}Ar at a bombarding energy of 600 MeV have been measured. Components corresponding to sequential emission from two fully accelerated reaction fragments as well as preequilibrium neutron emission have been separated as a function of energy loss and fragment atomic number. The deduced division of total excitation energy between the reaction partners is very well described by the one-body nucleon-exchange model for all energy losses. The data provide no evidence for correlations between the excitation energy division and the measured projectile-like fragment atomic number.

I. INTRODUCTION

The topic of excitation energy relaxation in mass-asymmetric damped heavy-ion reactions has received a great deal of attention over the past few years. Several studies[1-13] have concluded that in damped heavy-ion (HI) collisions of a few MeV per nucleon above the Coulomb barrier, the two reaction fragments are often produced with different temperatures. This experimentally determined thermal disparity indicates that equilibrium is usually not achieved during the dinuclear interaction phase. Certain experiments[1-7] conclude that the division of excitation energy between the two reaction fragments depends on the interaction time (energy loss) of the dinuclear system. For collisions with short interaction times, the excitation energy is shared almost equally between the two reaction products. As the interaction time increases, however, the heavy nucleus begins to receive more excitation energy. In this way, the dinuclear system approaches thermal equilibrium.

This observed trend in the excitation energy division is in qualitative agreement with the predictions of the one-body nucleon-exchange model (NEM) proposed by Randrup.[14,15] In this model, the redistribution of the excitation energy is mediated by the exchanged nucleons which deposit energy mainly in the recipient nucleus. In the initial stages of the reaction, there is no preferred direction of mass flow, so on average, the nuclei share equally in the excitation energy. For mass-asymmetric systems, this equal energy sharing leads to a thermal disparity between the reaction fragments. The temperature gradient thus established will, if the dinucleus lives long enough, drive the system to thermal equilibrium.

The assumption that the exchanged nucleons mediate the redistribution of the excitation energy is supported by studies[8-11] of the excitation energy division in quasielastic heavy-ion collisions. The results of these experiments indicate that, for reactions involving the exchange of only one or two nucleons, the recipient nucleus is significantly hotter than the donor nucleus. In further support of the NEM, the measured[7] excitation energy division between collision partners in the ^{139}La+^{40}Ar reaction at $E_{\mathrm{lab}}=400$ MeV is well described by the NEM for all energy losses. This agreement implies that the underlying microscopic mechanisms considered in the model are largely responsible for the exchange of excitation energy in a damped nuclear reaction.

Since the NEM assumes that the exchanged nucleons are the mediators of the excitation energy redistribution, it may seem reasonable to assume that in damped reactions, the division of excitation energy between the two reaction fragments should be correlated with the final mass of those fragments. This, however, is not the case in the framework of the NEM, because the net number of nucleons transferred to a particular fragment in a damped collision is usually quite small as compared to the number of nucleons actually exchanged. There are some experimental studies,[6,12,13] however, that report a strong correlation between the excitation energy division and the net mass transfer in a damped reaction for a fixed energy loss. The conclusions that have been drawn from these experiments are at variance with the predictions of the NEM, which allows only for weak mass-energy correlations of this type. The model was very successful[7] in reproducing the experimentally determined excitation energy division for all energy losses in the ^{139}La+^{40}Ar reaction at $E_{\mathrm{lab}}=400$ MeV. In order to study the bombarding energy dependence of the energy relaxation mechanism as well as to shed some light on the apparent discrepancy between the results discussed above, another experiment was performed on the same system at a laboratory bombarding energy of 600 MeV. This elevated bombarding energy will cause more violent collisions, as well as increase the range of available kinetic energy that can be dissipated in the collision. This will provide further stringent tests on the ability of the NEM to reproduce the experimentally determined excitation energy division. Table I lists a few of the relevant reaction parameters for the ^{139}La+^{40}Ar reaction at $E_{\mathrm{lab}}=600$ MeV.

The experimental procedure will be detailed in Sec. II,

TABLE I. Characteristic reaction parameters for the system $^{139}_{57}La+^{40}_{18}Ar$ at $E_{lab}=15.0$ MeV per nucleon.

Composite system: $^{179}_{75}Re$
Reduced mass $\mu=31.1$ u
Strong-absorption radius $R_{sa}=12.5$ fm
Coulomb energy $V_c(R_{sa})=118.5$ MeV
Bombarding energy $(E_{c.m.}-V_c)/\mu=11.2$ MeV per nucleon
Grazing angle $\theta_{1/4}^{lab}=13°$
Grazing angular momentum $l_{max}=280\ \hbar$
Total reaction cross section $\sigma_R=3.6$ b
Maximum fusion angular momentum $l_{crit}=109\ \hbar$
Fusion cross section $\sigma_{fus}=0.6$ b
Liquid-drop limit of stability $l_{RLDM}=82\ \hbar$
Interaction time for damped collisions $t_{int}\simeq 5\times 10^{-22}$ s

and the results of the experiment will be presented in Sec. III. A discussion of these results follows in Sec. IV, and the conclusions of this work are summarized in Sec. V.

II. EXPERIMENTAL PROCEDURE

A schematic diagram of the experimental setup is given in Fig. 1. A beam of 600-MeV ^{40}Ar particles, produced by the Lawrence Berkeley Laboratory 88-in. Cyclotron, bombarded a self-supporting 500-μg/cm^2 ^{139}La target that was placed in a spherical, 51-cm diameter, stainless-steel scattering chamber with 1.6-mm wall thickness. The beam dump was heavily shielded with paraffin in order to reduce the background of neutrons produced by the beam in the Faraday cup. A silicon solid-state detector telescope was placed at a laboratory angle of $\theta_{HI}=-10°$, approximately 18 cm away from the target. This laboratory angle is 3 deg forward of the grazing angle for projectile-like fragments (PLF's) (see Table I). Heavy ions that recoil near the grazing angle are expected to span a wide range of energy loss; therefore, the placement of the solid-state detector allows a sampling of many interaction times. The detector was comprised of a 75-μm-thick transmission detector in front of a 200-μm-thick stop detector and was used to detect the projectile-like fragments from the damped reaction. Seven neutron time-of-flight (TOF) detectors were placed at various angles between 100° and −100° about the target chamber in the plane of the heavy-ion telescope. The five backward-angle detectors were approximately 100 cm away from the target, while the two forward detectors were 150 cm away. The detectors consisted of 5-in. diameter by either 1.5- or 2.0-in.-thick NE213 liquid scintillators backed by Amperex 2041 photomultiplier tubes. Anticoincidence detectors ("proton paddles") consisting of thin plastic scintillators viewed by RCA photomultiplier tubes were placed in front of the five most forward neutron detectors, in order to detect high-energy charged particles that were able to escape the scattering chamber.

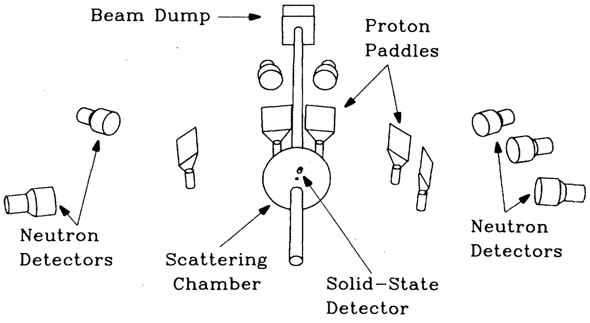

FIG. 1. Schematic diagram of the experimental setup.

A start signal for the neutron TOF was derived from the silicon solid-state telescope, while the neutron detectors provided stop signals. The time between the start and stop signals, differing from the true neutron TOF by the TOF of the heavy ion, was measured with a time-to-digital converter (TDC). The experimental time resolution was 0.60 ns for γ rays in coincidence with quasielastic events. Pulse-shape discriminators developed at the Hahn-Meitner Institut (Berlin) provided efficient neutron-γ selection. The proton recoil energy (scintillator light output) was also measured with these neutron detectors, and a threshold of approximately 0.5 MeV was set on this spectrum. All events, including elastic scattering, were recorded event by event.

In Fig. 2, the TOF spectra of events identified as neu-

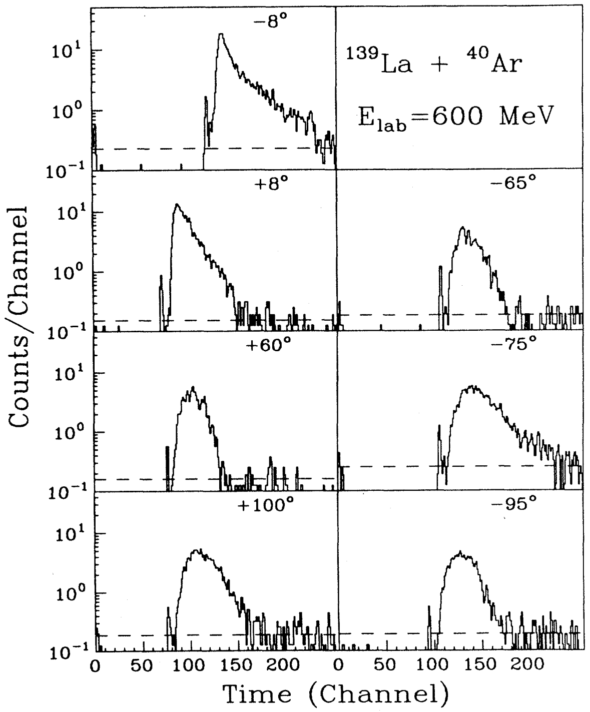

FIG. 2. Time-of-flight spectra for all neutron detectors coincident with PLF's detected at $\theta_{HI}=-10°$. The numbers in the upper right-hand corners refer to the detector angles θ_n, and the dashed lines illustrate the beam-related background subtracted before the conversion to energy.

trons by the pulse-shape discrimination system are shown for all neutron detectors. These spectra are not yet corrected for the TOF of the PLF. The main feature of each spectrum is a broad bump due to neutrons and a sharp peak at small times corresponding to the γ rays that were admitted with low probability by the pulse-shape discrimination system. The discriminators were intentionally set to allow this weak "leak through" of γ rays, in order to ensure that very few neutrons were incorrectly identified as γ rays.

The neutron detector placed at −8° is closest to the PLF's direction of flight; therefore, it sees the highest-energy (lowest-TOF) neutrons. The sharp cutoff at long times seen in all detectors except those at −8° and −75° is due to the threshold set in the experiment. For most detectors, the threshold was set close to 0.5 MeV. It is obvious from the figure that the thresholds for the detectors at −8° and −75° are lower than the others, while the threshold for the 60° detector is higher. Thresholds were measured before and after the experiment, and there was no change between these two measurements. The dashed lines represent the background level that was subtracted before converting the TOF to energy. The level of this background was determined by averaging the number of counts at long times (times that correspond to energies that are much lower than the measured threshold). In all cases, this is less than 0.3 counts per channel. This horizontal background is obviously an idealization. Close examination of Fig. 2 reveals that there are very few background neutrons detected before the first γ rays reach the scintillator. The background increases significantly, however, at long times. The background, then, is beam related, and the horizontal line subtracted from the spectra is only an estimate of the true background that was present during the experiment. The effect of subtracting a variety of different background levels was investigated, and it was determined that the only significant effect was a change in the high-energy tails of the neutron spectra. This small ($\sim 1\%$) systematic error is included in the analysis.

Another source of systematic error in this experiment is the finite-time resolution of the detector system, which was 0.60 ns for γ rays in coincidence with quasielastic events. This corresponds to an energy resolution of 2.4–3.6 % (depending on detector distance) for 5-MeV neutrons, and 7.4–10.8 % for 50-MeV neutrons. The detectors at ∓8°, which see the highest-energy neutrons, have the best resolution because they were the farthest away from the target.

The two-dimensional scatter plot in Fig. 3 shows the light output of the scintillator versus the neutron TOF (not corrected for the PLF TOF) for a typical neutron detector. The vast majority of events falls in the correctly correlated region, with long flight times corresponding to low proton recoil energies, and vice versa. The uncorrelated events were disregarded in the final analysis.

III. EXPERIMENTAL RESULTS

The energies deposited by the reaction fragments in the solid-state transmission and stop detectors were converted on an event-by-event basis to PLF atomic number (Z) and laboratory kinetic energy (corrected for pulse-height defect). The results of this conversion are shown in Fig. 4 where the (post-evaporation) Z is plotted vs PLF kinetic energy. The elastic peak at approximately 600 MeV is evident, as is the excellent resolution of the solid-state telescope of these energies. This figure indicates a strong drift in atomic number to lower Z's as the PLF energy

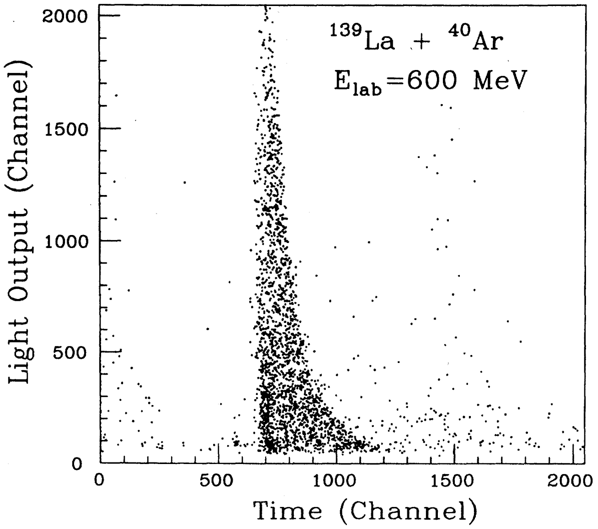

FIG. 3. Scatter plot of light output versus time of flight for neutrons detected at +8°.

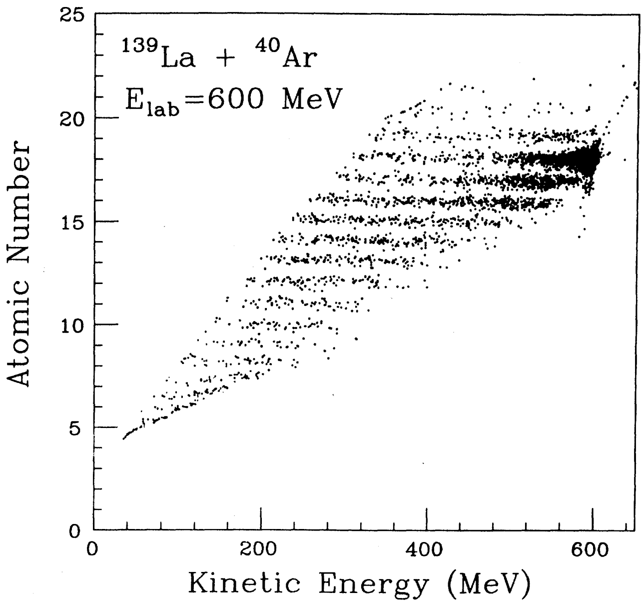

FIG. 4. Scatter plot of PLF atomic number vs PLF laboratory energy, indicating the excellent resolution of the solid-state telescope.

decreases (energy loss increases). As energy loss increases, however, the amount of evaporation of particles from the excited primary fragment increases, diluting the effect of a drift induced by nucleon exchange. Thus, conclusions about the nucleon-exchange process cannot be drawn from this figure alone.

The energy loss or reaction Q value, as well as the velocity of the target-like fragment (TLF) were calculated iteratively from the detection angle, charge, and the energy of the secondary PLF, as detailed elsewhere.[7] The PLF velocity was used to correct the measured neutron TOF. The correction amounted to a few ns, depending on the kinetic energy of the PLF. The resulting neutron TOF was then converted to energy on an event-by-event basis, and the measured intensity was divided by the neutron detector efficiency. The efficiency, which depends on neutron energy, scintillator geometry, and detector threshold, was calculated using the Monte Carlo program of Del Guerra,[16] modified by Cecil *et al.*[17] The results of this transformation are shown in Fig. 5 for neutrons coincident with PLF's for all Z values and total kinetic-energy losses of 20 MeV or higher. The error bars on the measured points are a sum of statistical errors and the error introduced by the background subtraction.

The solid curves in the figure are the results of a two-source fit which attempts to describe the data in terms of neutron emission from only the two fully accelerated reaction fragments, emitting isotropically in their rest frames. The energy spectrum of neutrons evaporated isotropically in the rest frame of emitter ν is assumed to be[7]

$$\frac{d^2\overline{m}_\nu}{d\Omega\, dE}=\frac{\overline{m}_\nu}{2}(\pi T_\nu)^{-3/2}E^{1/2}\exp(-E/T_\nu)\ , \qquad (1)$$

where $\overline{m}_\nu$ is the average multiplicity of neutrons from emitter ν (ν=PLF or TLF), T_ν is a parameter determining the slope of the energy spectrum, and E is the neutron energy in the emitter's rest frame. Converting from the emitter rest frame to the laboratory frame, the laboratory energy spectrum of neutrons from emitter ν becomes[7]

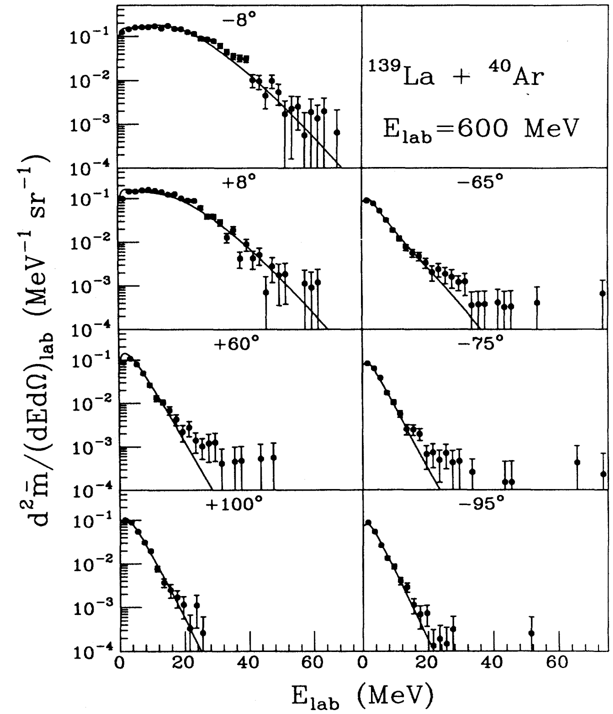

FIG. 5. Laboratory energy distributions for all neutron detectors. The solid curves represent a two-source fit, taking into account emission from the PLF and TLF.

$$\frac{d^2\overline{m}_\nu}{(d\Omega\, dE)_{\rm lab}}=\frac{\overline{m}_\nu}{2}(\pi T)^{-3/2}E_{\rm lab}^{1/2}\exp\{-[E_{\rm lab}-2(\epsilon_\nu E_{\rm lab})^{1/2}\cos(\theta_\nu)+\epsilon_\nu]/T_\nu\}\ . \qquad (2)$$

Here, $E_{\rm lab}$ is the neutron laboratory energy, ϵ_ν is the energy per nucleon of emitter ν, and θ_ν is the laboratory emission angle relative to the emitter's direction of flight. The two-source fit was performed by simultaneously adjusting two functions given by Eq. (2) for all laboratory detection angles θ_n. Fixed average values of ϵ_ν and θ_ν were taken from the energy-loss conversion, while $\overline{m}_\nu$ and T_ν were allowed to vary, giving four free-fit parameters. The results of this fit are illustrated by the solid curve in Fig. 5. Close examination of the figure reveals that the data are well described at forward and backward angles, where emission from the PLF and TLF, respectively, dominate. However, at intermediate angles, the spectra exhibit a high-energy component that is not described by the two-source fit.

In order to describe this high-energy component, a third, hypothetical source, moving in the direction of the beam, was added to the fit. For simplicity, the spectral shape of neutrons from this source was also assumed to be of the form given by Eq. (2). The multiplicity, slope parameter, and energy per nucleon were allowed to vary, making a total of seven free-fit parameters. The results of this fit are shown in Fig. 6, where the dotted curve represents the neutrons emitted by the TLF, the dashed curve represents neutrons emitted by the PLF, and the dot-dashed curve is the result for neutrons emitted by the third source. The solid curve is the sum of the neutron components from all three sources. It is evident that this fit is a much better representation of the data for all angles than the two-source fit, improving the value of chi square by about 50%. The properties of the neutron distributions summarized by the hypothetical third emission

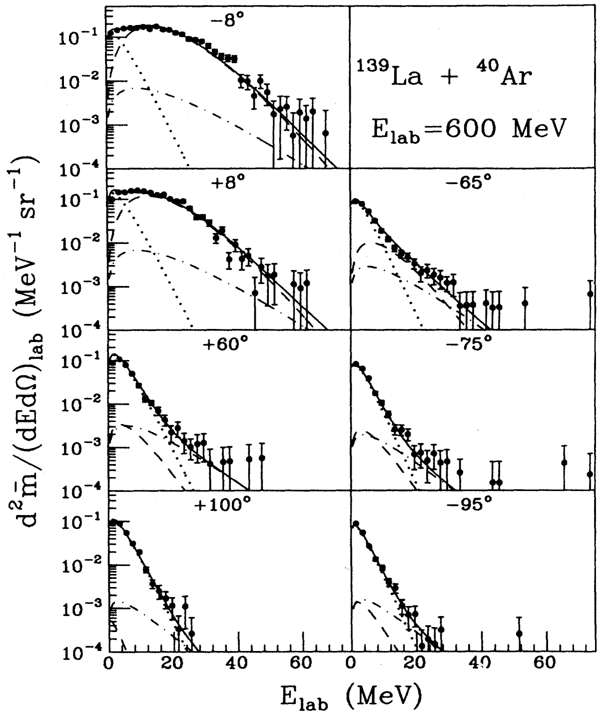

FIG. 6. Laboratory energy spectra for all neutron detectors. The solid curves represent a three-source fit, taking into account emission from the PLF (dashed curves), TLF (dotted curves), and a preequilibrium source (dot-dashed curves).

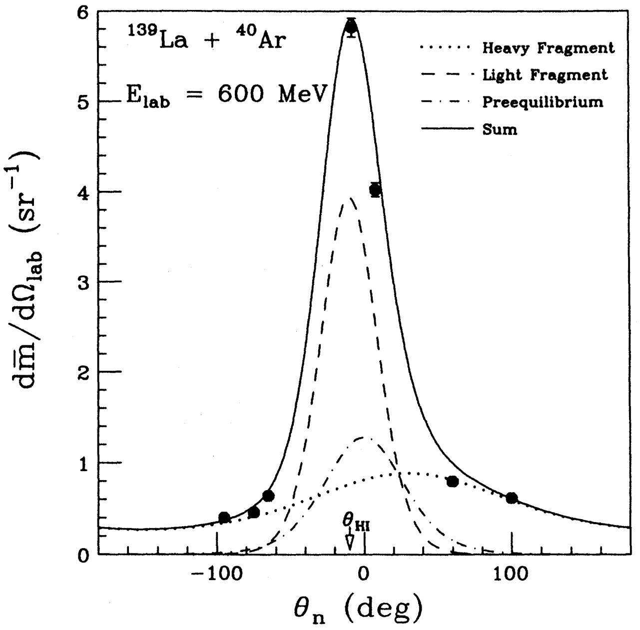

FIG. 7. Neutron laboratory angular distribution. Circles are the data, while the solid curve is the sum of TLF (dotted curve), PLF (dashed curve), and preequilibrium (dot-dashed curve) components derived from a three-source fit.

source are consistent with the phenomenon of preequilibrium neutron emission, as discussed elsewhere.[18]

Figure 7 shows the angular distribution of neutrons in the laboratory reference frame. The circles with error bars are the integrals of the neutron-energy spectra in Figs. 5 and 6 for each angle. The curves represent the expected angular distributions for neutrons evaporated from the three sources, obtained by integrating Eq. (2) over all angles. It can be seen from the figure that the emission pattern of neutrons from the slow-moving TLF (dotted curve) is almost isotropic in the lab, while the neutrons from the fast-moving PLF (dashed curve) are strongly focused in the PLF detection angle ($\theta_{HI} = -10°$). This neutron component has a much larger intensity than that from the preequilibrium source (dot-dashed curve) for all angles except +60°, making data obtained for this detection angle the most sensitive to preequilibrium emission. The solid curve in Fig. 7, the sum of all three components, clearly describes the data quite well for all angles. It is also evident from the figure that an angular distribution alone is not sensitive enough to detect preequilibrium neutron emission in this reaction. Only by simultaneously measuring both the energy and angle of the neutrons can preequilibrium emission be detected.

Because of the relatively high bombarding energy in this experiment, calculations were performed to estimate the percentage of neutrons that are emitted before the reaction fragments reach their asymptotic velocities. For this estimate, the spectrum of neutron emission times is assumed to fall exponentially as a function of time with a decay constant given by the mean evaporation time[19,20]

$$t_n = \frac{m}{2} e^{(13\ \mathrm{MeV}/\tau)} 10^{-22}\ \mathrm{s}\ , \qquad (3)$$

where τ is the nuclear temperature in MeV. Such a dependence of the characteristic evaporation time on temperature has been deduced from decay widths of compound nuclei produced at relatively low excitation energies. Its application to the present case of strongly damped reaction fragments requires a significant extrapolation of Eq. (3) which may be justified, however, for the purpose of estimating a small correction. An acceleration time calculated in the framework of the NEM was used to provide limits of integration for the emission time spectrum. The percentage of neutrons emitted before the PLF attains 90% of its asymptotic velocity was found in such a calculation to increase from 3%, at low-energy losses, to 20%, for the most strongly damped events. The average velocity at which the neutrons are emitted ranges from 99% of the asymptotic PLF velocity, at low-energy losses, to 83%, for events with large amounts of kinetic-energy damping. This causes a small uncertainty in the source fits discussed above, which is well within the experimental limitations.

It has been demonstrated that the data are consistent with three sources emitting isotropically in their rest frames. Hence, it is possible to convert the data from the laboratory to the emitter rest frames, in order to be able to increase the statistical accuracy of the spectra by averaging over all detection angles. This conversion was accomplished for each desired energy-loss bin using an event by event, iterative method described previously.[7] The results of this transformation are shown in Fig. 8 where the double-differential multiplicity of neutrons, averaged over fragment Z values and energy loss as before, is plotted versus the neutron center-of-mass (rest frame) energy E. The spectra correspond to neutrons from the PLF (circles) and the TLF (squares) as measured at the indicated laboratory neutron angles. The solid curves are the results of fits to the data performed with Eq. (1). At backward angles, the deviation between the data and the theoretical spectra for low-energy neutrons from the PLF is due to kinematic cutoffs in the laboratory system, caused by the large PLF velocity. This effect is also noticeable for neutrons from the TLF, although the effect is much smaller because of the low-TLF velocity. The data indicate that the neutrons are evaporated isotropically in the emitter rest frame. It is also evident from Fig. 8 that the slopes of the neutron-energy spectra associated with the PLF and TLF are different from each other.

Figure 9 shows the energy spectra of neutrons from the preequilibrium source in the asymptotic nucleon-nucleon rest frame, since the laboratory fits had indicated that the velocity of this source was approximately equal to one-half of the beam velocity. At backward angles, a kinematic cutoff induced by this velocity is also evident for neutrons from this component, as in the case of emission from the PLF. Neutrons from the preequilibrium source have on average higher energy than the neutrons from the fully accelerated reaction fragments, and it is also assumed that these neutrons are emitted during the approach phase of the collisions. Therefore, in the energy-loss calculation, a correction must be taken into account for the amount of energy taken away from the dinuclear system by preequilibrium emission. Such a correction is included in all of the figures presented.

Finally, neutron spectra from each emission source were grouped according to energy loss, and averaged over detection angle. Because of the kinematic cutoffs at backward angles, the spectra of neutrons from the PLF were only averaged over the detection angles of +8° and −8°. Since the kinematic cutoff effect is not large for neutrons from the TLF, the corresponding spectra were averaged over all detection angles. The results of this averaging are shown in Fig. 10 where the double-differential neutron multiplicity for various energy-loss bins is plotted versus neutron energy in the rest frames of the PLF (circles) and the TLF (squares). The solid curves are the respective fits for each source using Eq. (1). As energy loss increases, multiplicity and slope parameter in-

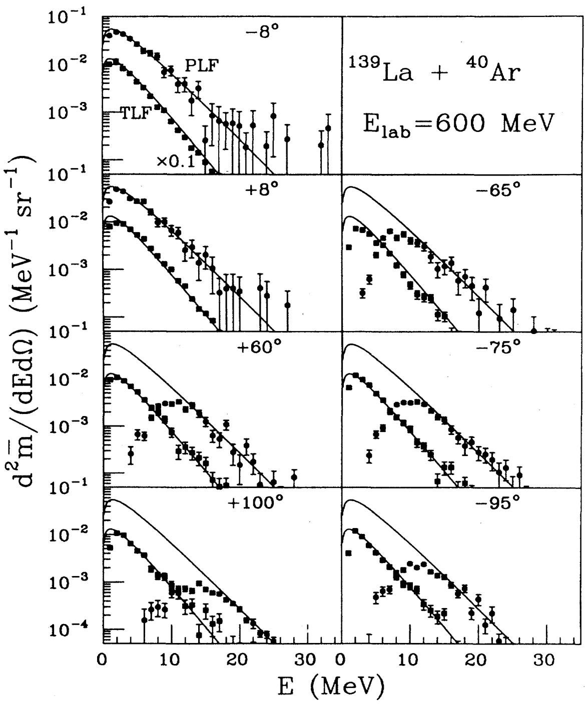

FIG. 8. Neutron-energy spectra in the rest frames of the PLF (circles) and TLF (squares). The intensity of neutrons from the TLF is divided by 10 for viewing purposes. The angles in the upper right-hand corners refer to laboratory detection angles. Each solid curve represents a fit to the corresponding spectrum with Eq. (1).

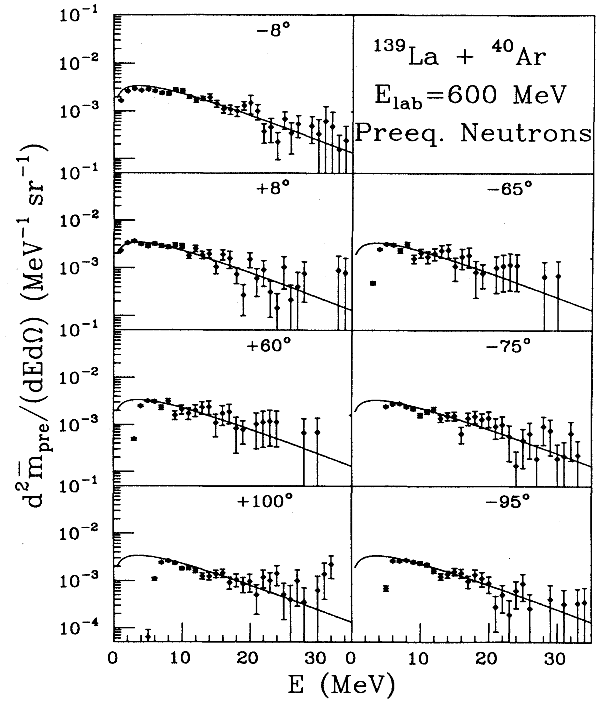

FIG. 9. The energy spectra of preequilibrium neutrons in the asymptotic nucleon-nucleon rest frame. The angles in the upper right-hand corners refer to laboratory detection angles. Diamonds represent the data, while the solid curves are fits with Eq. (1).

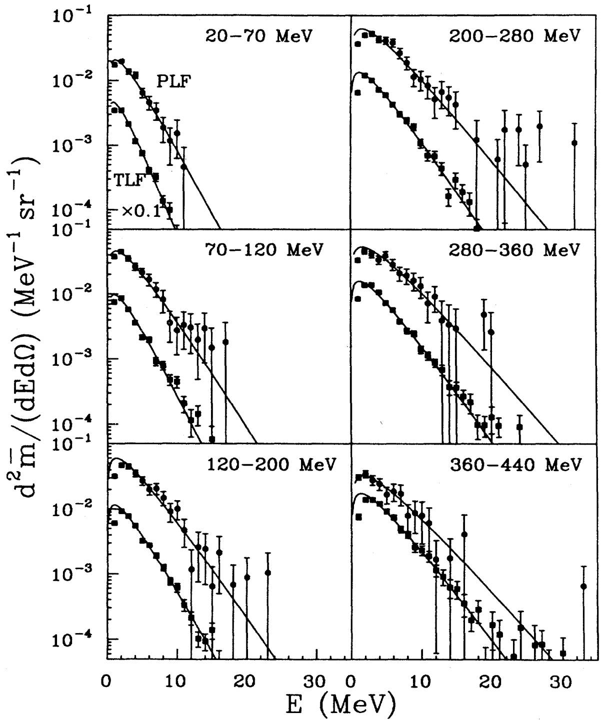

FIG. 10. Energy distributions of neutrons from the PLF (circles) and TLF (squares), in their respective rest frame of the emitters for several energy-loss bins. The intensity of neutrons from the TLF is divided by 10 for viewing purposes. The solid curves are fits with Eq. (1).

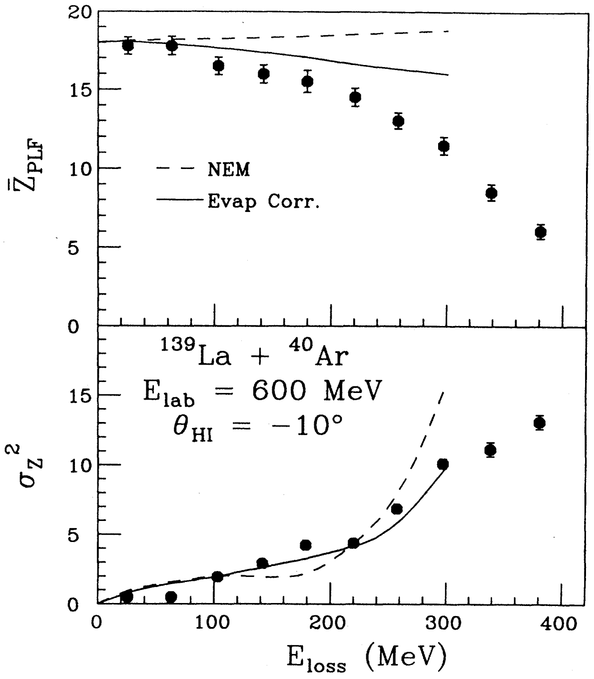

FIG. 11. The measured first and second moments of the PLF atomic number distribution compared to the predictions of the NEM. The dashed curves represent the NEM predictions prior to evaporation, while the solid curves are the result of a detailed evaporation calculation.

crease for both the PLF and TLF spectra, as expected. However, the slopes of the energy spectra of neutrons from these two sources differ for all values of energy loss. As has been demonstrated previously,[1] this is not necessarily a sign of nonequilibrium energy sharing, as the slope parameters have no simple relationship to the nuclear temperatures of the primary reaction fragments.

IV. DISCUSSION

As mentioned previously, the NEM has been successful in reproducing the excitation energy division observed in a previous experiment using the same projectile-target combination.[7] Thus, it is desirable to compare the present data to the NEM as well. Figure 11 shows the first and second moments of the measured PLF element distribution as a function of energy loss. The dashed curves are the predictions of the NEM for primary reaction fragments, whereas the solid curves include a correction for evaporative decay of these fragments, calculated as described below. According to the model, the primary PLF should acquire on average up to one proton, as the energy loss approaches large values, a gain that is overcompensated by evaporative loss. Close examination of the figure reveals that the trend of the first moment of the element distribution is reasonably well reproduced, although the strength of the drift toward lower Z's is not quantitatively described. The description of the second moment by the NEM, however, is quite good. This result is a rather interesting observation in itself, suggesting the dominance of the one-body reaction mechanism at elevated bombarding energies of at least 15 MeV per nucleon.

Figure 12 demonstrates the success of the NEM in reproducing the measured excitation energy division in this reaction. The ratio $T_{\mathrm{TLF}}/T_{\mathrm{PLF}}$ of the measured slope parameters T_ν of the neutron-energy spectrum for neutrons from the TLF and the PLF [Fig. 12(a)] as well as the ratio $\bar{m}_{\mathrm{TLF}}/\bar{m}_{\mathrm{PLF}}$ [Fig. 12(b)] of the corresponding multiplicities are plotted versus energy loss for the $^{139}\mathrm{La}+{}^{40}\mathrm{Ar}$ reaction at $E_{\mathrm{lab}}=600$ MeV. The error bars on the measured points are a sum of statistical and systematic errors. The systematic error is mainly due to the finite-time resolution of the detector system, as discussed previously.

The curves in Fig. 12 are the results of detailed statistical evaporation calculations involving the computer code PACE.[21] The calculations were performed in the following manner: for each energy-loss bin, primary projectile-like and target-like fragment distributions were calculated using the one-body nucleon-exchange model. Then, a PACE calculation was performed for each fragment in this distribution. The assumptions that must be made at this point in the calculation are twofold. Firstly, the parameters governing the statistical decay of the nuclei must be assumed. Except for the level-density parameter a (discussed below), all values for the statistical parameters

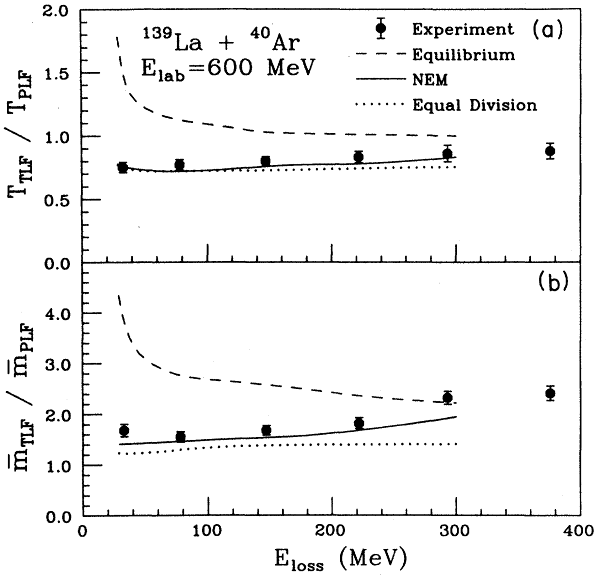

FIG. 12. The ratios of the deduced slope parameters T_{TLF}/T_{PLF} and multiplicities $\overline{m}_{TLF}/\overline{m}_{PLF}$ of neutrons from the TLF and the PLF. The circles are the data, and the curves illustrate the results of detailed statistical calculations explained in the text.

were taken from systematics.[21] The second assumption refers to how the available excitation energy is divided between the reaction fragments. The calculation was performed for three different assumptions: thermal equilibrium (dashed curve), equal energy division (dotted curve), and the division given by the NEM (solid curve). Additionally, in damped nuclear reactions, for a fixed energy loss, the distribution of excitation energies generated in each fragment must have a finite width. In the calculations shown in Fig. 12, the excitation energy distribution for each fragment was assumed to be Gaussian, with a width given by equilibrium conditions.[22] Such a width is likely to represent a lower limit to the actual energy fluctuation, but is used here, lacking a better estimate. In order to assess the associated uncertainties, calculations were also done assuming widths as large as three times the equilibrium widths. They demonstrated a rather weak dependence of the average theoretical quantities displayed in Fig. 12 on the magnitude of these widths, with variations well inside the experimental uncertainties. For each fragment nuclide and energy-loss bin, five PACE calculations were performed using different points along the assumed excitation energy distribution (one at the maximum, two at half maximum, and two at 15% of the maximum). The PACE calculations were performed neglecting the relatively small effect of fragment spin[1] and with a level-density parameter of

$$a_{PLF}=(A_{PLF}/8)\ \mathrm{MeV}^{-1}$$

for the PLF and

$$a_{TLF}=(A_{TLF}/12)\ \mathrm{MeV}^{-1}$$

for the TLF. The motivation for using these values of a has been discussed in an earlier work.[7] The resulting neutron-energy distributions and multiplicities were then integrated according to the theoretical abundance of the primary reaction fragment and the relative probability on the excitation energy distribution, and the final neutron-energy spectra were fit with Eq. (1). The result of such a long and complicated calculation is a detailed statistical prediction of the neutron-energy distributions and multiplicities for a damped heavy-ion reaction, for each assumed excitation energy division.

In both Figs. 12(a) and 12(b), a comparison of the data to the statistical predictions indicates that at low-energy losses (small reaction times), each fragment gets nearly 50% of the total excitation energy, and, as the energy loss (reaction time) increases, the TLF begins to receive more excitation energy, approaching the equilibrium limit. For all energy losses, however, the predictions of the NEM fit both sets of data very well, in agreement with previous results[7] for the same projectile-target combination at a lower bombarding energy of 400 MeV, and with those of earlier work.[3–6] Thus, for two different bombarding energies, the measured excitation energy division is well reproduced for all interaction times by the NEM for the system ^{139}La+^{40}Ar.

One additional point can be made about the excitation energy relaxation process from a comparison between the two experiments discussed above. Averaged over all energy losses greater than 20 MeV, the preequilibrium neutron multiplicity was

$$\overline{m}_{pre}=(0.11\mp0.03)$$

in the 400-MeV reaction, but it rose to

$$\overline{m}_{pre}=(0.71\mp0.04)$$

for a bombarding energy of 600 MeV. Although the preequilibrium neutron multiplicity has increased substantially between 400 and 600 MeV, the NEM's ability to reproduce the excitation energy division seems to be unaffected. As mentioned previously, the preequilibrium neutrons are assumed to take energy away during the early interaction phase, an effect that has been taken into account in the energy-loss conversion. It is important to emphasize that there is no need to modify the model in any way to account for preequilibrium emission, implying that preequilibrium emission occurs early in a collision and that, hence, its only effect on energy redistribution consists of a reduction of the total excitation energy introduced into the dinuclear system. The implications of the present experiment on preequilibrium emission will be discussed in a forthcoming publication.

As pointed out previously,[1,7] the effects of uncertainties in the assumed statistical parameters are reduced when the comparisons are made between ratios of the experimental and theoretical observables. However, it is also important to compare the NEM's predictions to the absolute multiplicities and slope parameters. In Fig. 13, the multiplicities $\overline{m}_{TLF}$ and $\overline{m}_{PLF}$ and the slope parameters T_{TLF} and T_{PLF} characterizing the neutron-energy spectra from each source are plotted versus energy loss.

The curves presented in the figure are the results of the same calculations discussed in the context of Fig. 12. It is quite clear from Fig. 13 that the NEM reproduces the absolute values of the data reasonably well, although the absolute predictions are susceptible to additional uncertainties associated with the statistical-model calculations.

One other experimental observable that can be examined, to further investigate the mechanisms governing the excitation energy relaxation, is the correlation between excitation energy and reaction fragment atomic number representing an average fragment mass. As mentioned previously, there are some experimental studies[6,12,13] claiming a strong correlation between the excitation energy division and the net mass transfer in a damped collision. For example, in a kinematic coincidence experiment,[6] on the damped reaction ^{165}HO+^{56}Fe at $E_{\mathrm{lab}}=504$ MeV, it was concluded that the excitation energy division depends linearly on the net mass transfer. It has been recently demonstrated,[23] however, that this correlation can be accounted for by a systematic error that was not considered in the data analysis.

Likewise, reports of strong correlations between the excitation energy division and the net mass transfer in a damped collision from radiochemical studies[12,13] must be viewed with caution due to the assumption of instantaneous A/Z equilibration made in the analysis. This assumption has been shown to be invalid for a number of projectile-target combinations at various bombarding energies.[24–26] Since the conclusions of the above studies are inconsistent with the predictions of the NEM, it is therefore interesting to explore the presence or absence of similar correlations in the ^{139}La+^{40}Ar reaction.

Figure 14 illustrates the behavior of the neutron multiplicities $\overline{m}_{\mathrm{TLF}}$ and $\overline{m}_{\mathrm{PLF}}$ and of the spectral slope parameters T_{TLF} and T_{PLF} as functions of PLF atomic number, for all events with an energy loss of 20–160 MeV. The bins in energy loss and PLF atomic number must be wide in order to have sufficient statistics to adequately define the shape of the neutron-energy spectra. Although the error bars on the individual data for the TLF (squares) somewhat overlap with those for the PLF, the trend is quite clear: The multiplicities and slope parameters of neutrons from both the TLF and PLF decrease with increasing PLF atomic number. If the excitation energy were actually correlated with the net mass transfer, the multiplicity and the spectral slope parameter of neutrons from one fragment should increase with increasing PLF Z while the corresponding data from the other source should decrease with increasing PLF atomic number. The data, however, do not exhibit such an anticorrela-

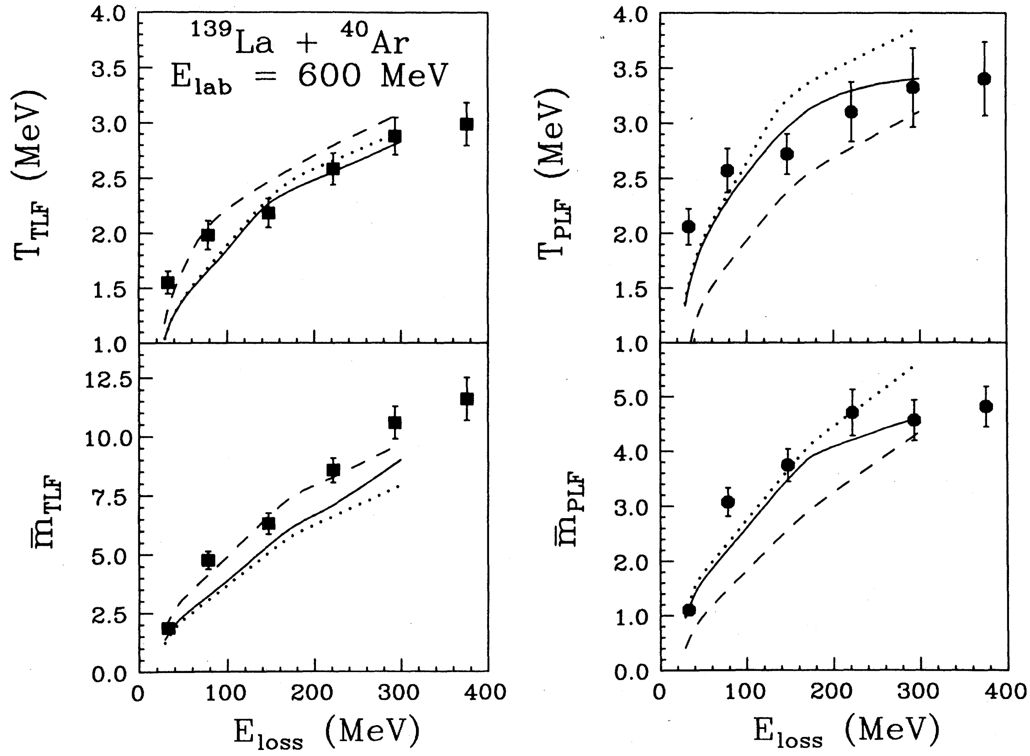

FIG. 13. The spectral slope parameters T_{TLF} and T_{PLF} and multiplicities $\overline{m}_{\mathrm{TLF}}$ and $\overline{m}_{\mathrm{PLF}}$ characterizing the energy spectra of neutrons from the TLF and PLF plotted versus energy loss. The curves represent detailed statistical calculations discussed in the text.

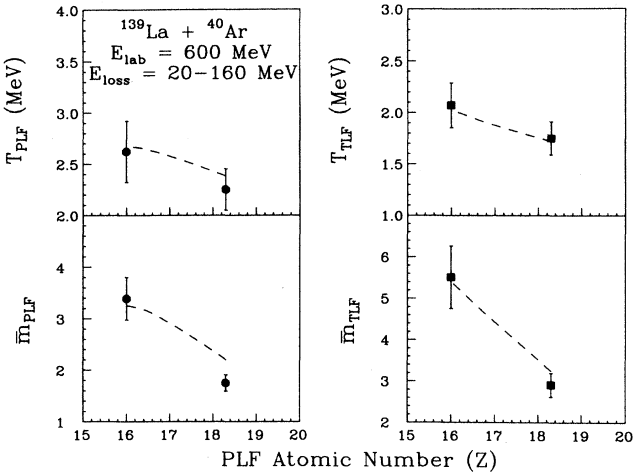

FIG. 14. The spectral slope parameters $T_{\rm TLF}$ and $T_{\rm PLF}$ and multiplicities $\overline{m}_{\rm TLF}$ and $\overline{m}_{\rm PLF}$ characterizing the energy spectra of neutrons from the TLF and PLF plotted versus the detected PLF atomic number. All data are coincident with energy losses between 20 and 160 MeV. The curves are explained in the text.

tion. Instead, the dependencies observed in the data can be easily explained in terms of the implicit energy-loss dependence of the fragment Z distribution over the width of the energy-loss bin. Within the given energy-loss bin of 20–160 MeV, for which the data are presented in Fig. 14, the larger values of the PLF atomic number correspond to lower-average energy losses because of the drift towards smaller average Z values with increasing energy loss (cf. Figs. 4 and 11). For events with a lower-average energy loss, the multiplicities and spectral slope parameters of neutrons from both sources must decrease (cf. Fig. 13), as seen in Fig. 14.

In order to illustrate this implicit energy-loss dependence, the average energy loss of events in each Z bin was calculated and the multiplicities and slope parameters expected for that energy loss were then estimated from an interpolation of the data shown in Fig. 13. The dashed curves in Fig. 14 represent the results of this interpolation. Figures 15 and 16 show the same correlation as Fig. 14 for two bins of higher-energy loss. In all cases, the data are consistent with the overall trend derived from Fig. 13, providing no positive evidence for a correlation between detected PLF atomic number and excitation energy division.

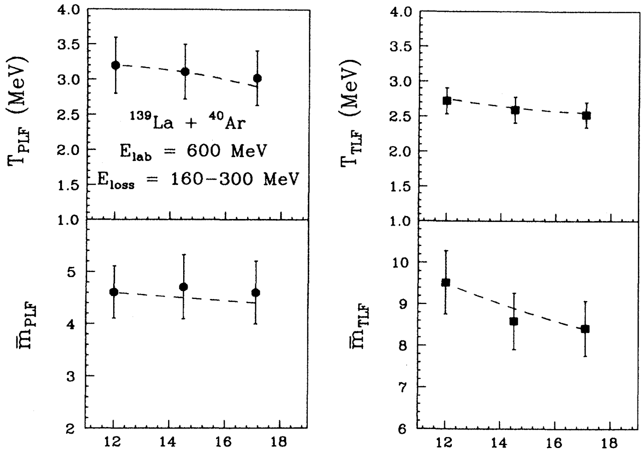

FIG. 15. Same as Fig. 14, except all data are coincident with energy losses between 160 and 300 MeV.

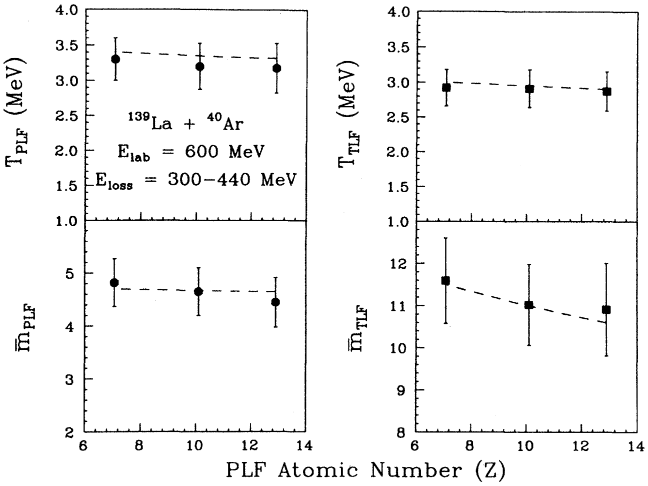

FIG. 16. Same as Fig. 14, except all data are coincident with energy losses between 300 and 440 MeV.

V. CONCLUSIONS

The present experimental results demonstrate that at a bombarding energy of 600 MeV, the intermediate dinuclear system in damped $^{139}\mathrm{La}+^{40}\mathrm{Ar}$ collisions does not survive long enough to equilibrate the available excitation energy. Instead, for all interaction times measured, the reaction products separate with different nuclear temperatures. For fast, partially damped collisions, the two reaction fragments share the excitation energy almost equally. As the interaction time increases, however, the heavy fragment begins to acquire a higher percentage of the excitation energy, approaching, but never reaching, the equilibrium limit. The time evolution of the excitation energy division is very well described by the NEM, in agreement with previous results[7] for the $^{139}\mathrm{La}+^{40}\mathrm{Ar}$ reaction at $E_{\rm lab}=400$-MeV reaction. These results suggest that in damped heavy-ion collisions even up to 15 MeV/nucleon, the energy relaxation processes are mediated by the one-body exchange of independent nucleons between the two reaction fragments. Additionally, no significant correlations between the excitation energy division and the final Z of the projectile-like fragment were observed, in agreement with the predictions of the NEM.

This work was supported by the U.S. Department of Energy under Grant No. DE-FG02-88ER40414.

[1] J. L. Wile, W. U. Schröder, J. R. Huizenga, and D. Hilscher, Phys. Rev. C **35**, 1608 (1987).

[2] J. R. Huizenga, W. U. Schröder, J. R. Birkelund, and W. W. Wilcke, Nucl. Phys. **A387**, 257C (1982).

[3] T. C. Awes, R. L. Ferguson, R. Novotny, F. E. Obenshain, F. Plasil, S. Pontoppidan, V. Rauch, G. R. Young, and H. Sann, Phys. Rev. Lett. **52**, 251 (1984).

[4] R. Vandenbosch, A. Lazzarini, D. Leach, D. K. Lock, A. Ray, and A. Seamster, Phys. Rev. Lett. **52**, 1964 (1984).

[5] L. G. Sobotka, G. J. Wozniak, R. J. McDonald, M. A. McMahan, R. J. Charity, L. G. Moretto, Z. H. Liu, F. S. Stephens, R. M. Diamond, M. A. Deleplanque, and A. J. Pacheco, Phys. Lett. B **175**, 27 (1986).

[6] D. R. Benton, H. Breuer, F. Khazaie, K. Kwiatkowski, V. E. Viola, S. Bradley, A. C. Mignerey, A. P. Weston-Dawkes, and R. J. McDonald, Phys. Lett. B **185**, 326 (1987).

[7] J. L. Wile, S. S. Datta, W. U. Schröder, J. R. Huizenga, J. Tõke, and R. T. de Souza, Phys. Rev. C **39**, 1845 (1989).

[8] K. Siwek-Wilczynska, R. A. Blue, L. H. Harwood, R. M. Ronningen, H. Utsunomiya, J. Wilczynski, and D. J. Morrissey, Phys. Rev. C **32**, 1450 (1985).

[9] H. Sohlbach, H. Freiesleben, P. Braun-Munzinger, W. F. W. Schneider, D. Schüll, B. Kohlmeyer, M. Marinescu, and F. Pühlhofer, Phys. Lett. **153B**, 386 (1985); Nucl. Phys. **A467**, 349 (1987).

[10] S. B. Gazes, H. R. Schmidt, Y. Chan, E. Chavez, R. Kamermans, and R. G. Stokstad, Phys. Rev. C **38**, 712 (1988).

[11] H. R. Schmidt, S. B. Gazes, Y. Chan, R. Kamermans, and R. G. Stokstad, Phys. Lett. B **180**, 9 (1986).

[12] H. Keller, R. Bellwied, K. Lützenkirchen, J. V. Kratz, W. Brüchle, H. Gäggler, K. J. Moody, M. Schädel, and G. Wirth, Z. Phys. A **328**, 255 (1987).

[13] H. Gäggler, W. Brüchle, M. Brügger, M. Schädel, K. Sümmerer, G. Wirth, J. V. Kratz, M. Lerch, Th. Blaich, G. Herrmann, N. Hildebrand, N. Trautmann, D. Lee, K. J. Moody, K. E. Gregorich, R. B. Welch, G. T. Seaborg, D. C. Hoffman, W. R. Daniels, M. M. Fowler, and H. R. von Gunten, Phys. Rev. C **33**, 1983 (1986).

[14] J. Randrup, Nucl. Phys. **A307**, 319 (1978); **A327**, 490 (1979).

[15] T. Døssing and J. Randrup, Nucl. Phys. **A433**, 215 (1985); **A433**, 280 (1985).

[16] A. Del Guerra, Nucl. Instrum. Methods **135**, 337 (1976).

[17] R. A. Cecil, B. D. Anderson, and R. Madey, Nucl. Instrum. Methods **161**, 439 (1979).

[18] J. L. Wile, S. S. Datta, W. U. Schröder, J. R. Huizenga, R. T. de Souza, and D. Pade (unpublished).

[19] R. G. Stokstad, in *Proceedings of the Topical Conference on Heavy-Ion Collisions, Fall Creek Falls State Park, Tennessee* (U.S. Department of Commerce, Washington, D.C., 1977).

[20] E. Holub, D. Hilscher, G. Ingold, U. Jahnke, H. Orf, and H. Rossner, Phys. Rev. C **28**, 252 (1983).

[21] A. Gavron, Phys. Rev. C **21**, 230 (1980).

[22] D. J. Morrissey and L. G. Moretto, Phys. Rev. C **23**, 1835 (1981).

[23] J. Tõke, W. U. Schröder, and J. R. Huizenga, Phys. Rev. C **40**, R1577 (1989).

[24] R. T. de Souza, J. R. Huizenga, and W. U. Schröder, Phys. Rev. C **37**, 1901 (1988).

[25] R. T. de Souza, W. U. Schröder, J. R. Huizenga, J. Tõke, S. S. Datta, and J. L. Wile, Phys. Rev. C **39**, 114 (1989).

[26] R. Planeta, S. H. Zhou, K. Kwiatkowski, W. G. Wilson, V. E. Viola, Jr., H. Breuer, D. Benton, F. Khazaie, R. J. McDonald, A. C. Mignerey, A. P. Weston-Dawkes, R. T. de Souza, J. R. Huizenga, and W. U. Schröder, Phys. Rev. C **38**, 195 (1988).